Radiative–Dynamical Consequences of Dry Tongues in the Tropical Troposphere

BRIAN E. MAPES AND PAQUITA ZUIDEMA

Program in Atmospheric and Oceanic Sciences, University of Colorado, Boulder, Colorado

(Manuscript received 10 April 1995, in final form 23 August 1995)

ABSTRACT

Dry layers are frequently observed in atmospheric soundings from the climatologically humid western Pacific warm pool region. Some 2400 soundings from the TOGA COARE field program were objectively examined for humidity drops (layers in which relative humidity decreases rapidly with height), indicative of the bases of dry layers. These occur throughout the lower and middle troposphere, with frequency peaks near 550 (the 0°C level), 800, and 950 mb.

A composite constructed from these sounding data indicates the following.

1) Almost all dry layers are too dry (and not warm enough) to be interpreted as conservative vertical displacements. Rather, they apparently consist of filaments or tongues of low moist static energy air advected into the column, often from the subtropics.

2) Dry tongues are anomalously virtually warm near their bases with a slight cool layer below; that is, they sit atop sharp stable layers or inversions.

The authors hypothesize that radiation is responsible for the thermal structure of dry tongues. The radiative effects of humidity structures in the troposphere are reviewed and illustrated. A composite-derived radiative heating perturbation, acting for 3.5 days in an idealized model of a dry tongue ~ 300 km in width (values consistent with case studies), reproduces fairly well the high vertical wavenumber components of the composite thermal structure. Dynamics acts to spread the effect of the radiative heating perturbation over a wider area and to concentrate the temperature perturbations near the dry tongue base, as observed. The deep layer-mean warmth of the composite dry tongue arises from a slight correlation between dry tongue occurrence in this dataset and a ~1°C global-scale intraseasonal variation of tropical tropospheric temperature.

A dry tongue affects convective clouds both directly, through its thermal structure, and indirectly, through dry air entrainment. Low-level dry tongues can prevent deep convection outright, while the stable layers associated with dry tongues at higher altitudes may cause convection to detrain mass. Humidity drops, stable layers, and a proxy for layer clouds all have similar altitude distributions.

1. Introduction

The temperature and moisture traces on atmospheric sounding plots frequently vary in opposition, indicating that dry layers tend to be warm, especially near their bases. This general tendency persists across a wide range of vertical scales, a wide range of amplitudes of temperature and humidity variation, and a wide range of altitudes in the atmosphere. Even in the climatologically moist and convecting atmosphere over the western Pacific Ocean, most soundings indicate one or more warm-dry layers in the atmosphere. Since these dry layers are not of infinite horizontal extent (often they are absent at even the nearest adjacent sounding sites), we refer to them as dry tongues.

One well-known, though rather rare, example of a warm dry layer is the "onion" sounding (Zipser 1977), frequently observed near and outside the stratiform rain regions of mesoscale convective systems. Onion soundings arise from adiabatic downward displacements in an otherwise quite humid atmosphere. The temperature and moisture traces are generally smooth and close together except at low levels, where they bulge apart, giving the sounding a shape like a green onion or scallion. Figure 1a shows a "double onion" (or "guitar") sounding. In this type of sounding, the warmth and dryness are commensurate, in the sense that both represent the same (typically ~ hundreds of meters) conservative vertical displacement of the ambient vertical gradients of specific humidity and potential temperature.

At another extreme are the very dry soundings observed at TOGA COARE[1] sounding sites on 11–13 November 1992 [Fig. 1b; also Fig. 5 of Parsons et al.

Corresponding author address: Dr. Brian E. Mapes, Program in Atmospheric and Oceanic Sciences, University of Colorado, Campus Box 311, Boulder, CO 80309.

[1] The Tropical Ocean Global Atmosphere program's Coupled Ocean–Atmosphere Response Experiment (Webster and Lukas 1992).

a) 0456 UTC 23 December (R/V Kexue 1)

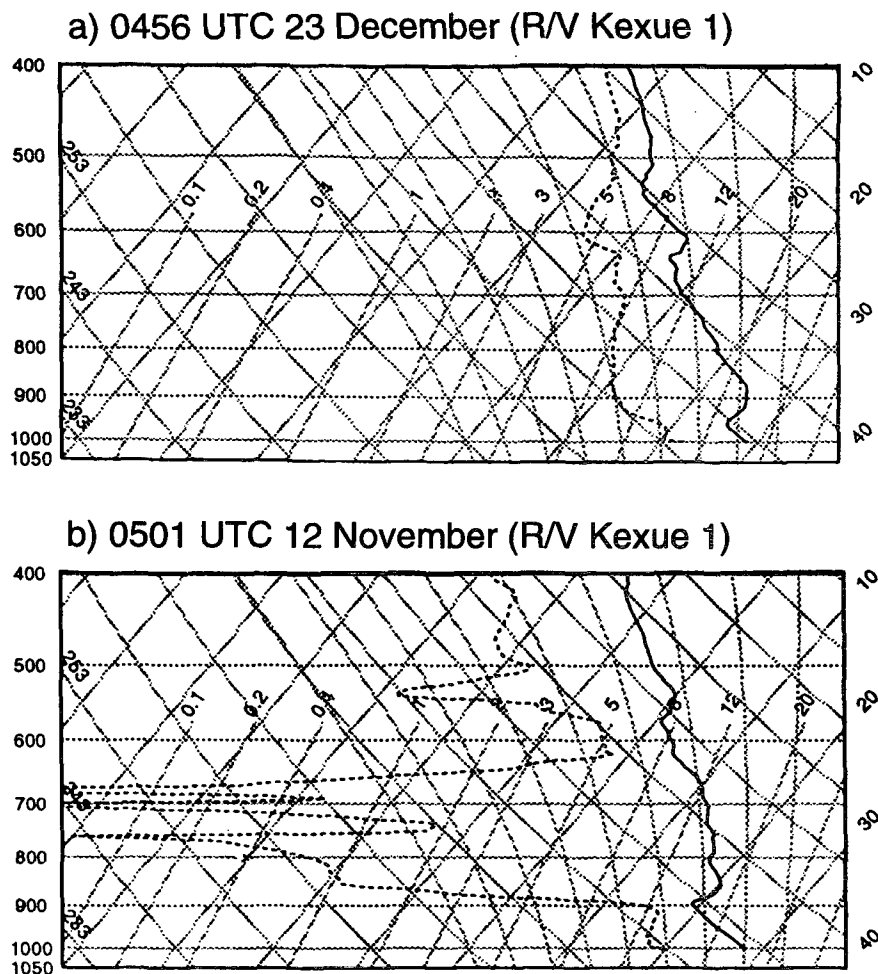### b) 0501 UTC 12 November (R/V Kexue 1)

FIG. 1. Two soundings with contrasting extreme cases of warm dry layers. (a) An "onion" sounding (Zipser 1977), characteristic of transient adiabatic vertical displacements in the vicinity of a mesoscale convective system. (b) A sounding with a low-level extremely dry tongue (from the site labeled "7" on Fig. 3). Both are plotted on skew T (labels at right, C) versus $\log p$ (labels at left, mb) charts, with mixing ratio lines labeled at their termini (g kg^{-1}) along the 550-mb level; solid: temperature, dotted: humidity.

(1994) and Fig. 8a of Numaguti et al. (1995)]. The soundings in Fig. 1 are plotted in Fig. 2 as profiles of moist static energy[2] h, a quantity approximately conserved during moist and dry adiabatic processes. The warm-dry layers from Fig. 1b (solid line) constitute strong, distinct minima of h, unlike the warm-dry layers from Fig. 1a (short dashed line). Since clear-air radiation generally tends to decrease h by about 1.5 kJ kg^{-1} day^{-1} (Fig. 12), Fig. 2 indicates that the very dry air mass near 850 mb, with its h deficiency of ~30 kJ kg^{-1} relative to surface and upper-tropospheric val-

ues, has undergone something like 20 days of radiative cooling since it was last in contact with a low-latitude sea surface. This is in sharp contrast to mean midtropospheric air (long dashes), with a similarly defined "radiative age" of just a few days.

Evidently the humidity structure in Fig. 1b did not result from adiabatic vertical displacements. A microwave satellite-derived precipitable water map (Fig. 3) shows that this sounding, at the position indicated by the plotted "7," sampled a narrow dry tongue protruding into the deep Tropics from the southern subtropics. Numaguti et al. (1995) studied this and another dry tongue using trajectory analysis and concluded that in both cases the dry air could be traced back to 20° latitude a few days earlier. Similar conclustions about the origins of other dry tongues during TOGA COARE

---

[2] Here $h = C_p T + gz + Lq$ (enthalpy + geopotential + latent heat content) is similar to equivalent potential temperature θ_e, with similar values when h is expressed in kJ kg^{-1} and θ_e in °K.
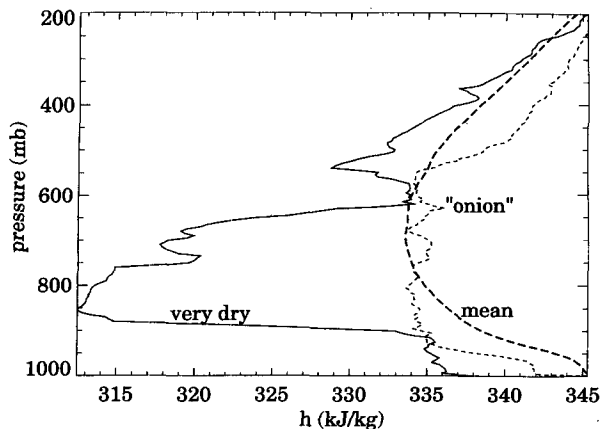
FIG. 2. Moist static energy profiles for the two soundings shown in Fig. 1 and for the mean sounding of Fig. 4a.

were reached by Yoneyama and Fujitani (1995) and Johnson et al. (1995). Clearly, horizontal advection is the proximate cause of the main dry layer in Fig. 1b. But why are both dry layers in Fig. 1b, at 700–900 and 550 mb, also warm?

This study is a statistical examination of more than 2400 soundings, collected at the eight near-equatorial sites in the western Pacific indicated on Fig. 3. The key feature studied here is the "humidity drop," a layer in which humidity decreases rapidly with height, indicative of the base of a dry layer. A composite analysis (section 3) shows that virtual temperature systematically jumps almost 0.4°C across these humidity drops. For the composite, as for Fig. 1b, the conservative vertical displacement that would be required to explain the dryness greatly exceeds values that could possibly be consistent with the composite warmth. The onion sounding of Fig. 1a therefore represents a practical upper limit to the magnitude of the temperature anomaly associated with dry tongues.

Since dry tongues are not merely adiabatic vertical displacements, another explanation for their thermal structure must be sought. The horizontally finite density perturbation is indicative of a dynamically active (baroclinic) situation. This observation and the pronounced diurnal cycle evident in the composite temperature structure (Fig. 8b below) are consistent with the idea that dry tongues cause nonnegligible perturbations to the radiative heating profile. Section 4 considers the effects of humidity on clear-air radiation profiles in the tropical troposphere. Section 5 illustrates how, given the composite humidity drop, the associated composite temperature structure can be explained as the result of clear-air radiation and dynamics acting for 3–4 days, which is the typical lifetime of dry tongues in the Tropics (Numaguti et al. 1995, Yoneyama and Fujitani 1995).

Dry-warm layers with sharp bases are sometimes referred to as "subsidence inversions." But the inade-

quacy of adiabatic subsidence in explaining many such layers was recognized by Namias (1936). He showed from observations that when dry air overlies moist, the interface tends to be anomalously stable, in terms of *virtual* temperature lapse rate, and discussed the possible influence of radiation in maintaining this thermal structure. However, the inaccuracies of both human-hair hygrometers and radiative transfer formulas of the time rendered his results less than conclusive. Staley and Jurica (1968) found that "in the vicinity of relatively dry inversions in the lower and middle troposphere, cooling rates were . . . so distributed as to maintain the inversion and substantially increase the hydrostatic stability in the lower part of the inversion." Sections 4 and 5 of the present study are essentially an extension of Staley and Jurica's results to the case of horizontally finite dry tongues.

The radiatively maintained stable layer at the base of a dry tongue may promote its longevity by inhibiting the development of penetrative buoyant convective clouds (section 6). Our discussion of this challenging issue is far from definitive. But convection is so central to tropical meteorological phenomena of every kind, and the reasons for its variability remain so unknown, that the effects of dry tongues on convective cloudiness remains a primary motivation for this study. When con-
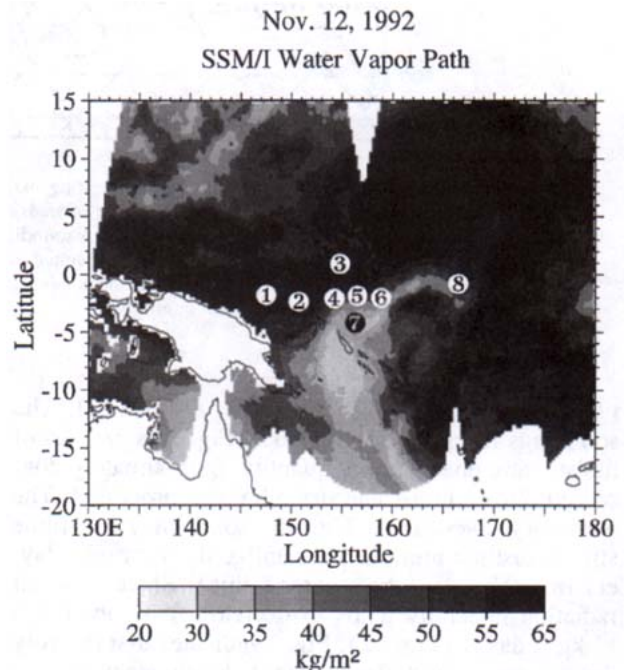

FIG. 3. Special Sensor Microwave Imager (SSMI)-derived column integrated water vapor, according to the Petty (1994) algorithm, for 12 November 1992 (a composite of multiple satellite overpasses). The eight stations used in this study are indicated by numbers: 1) Manus Island; 2) Kavieng; 3) Kapingamarangi Atoll; 4) R/V *Xiangyanghong* 5; 5) R/V *Moana Wave;* 6) R/V *Shiyan* 3; 7) R/V *Kexue* 1; and 8) Nauru.

a) Mean sounding

b) Mean u and v profiles

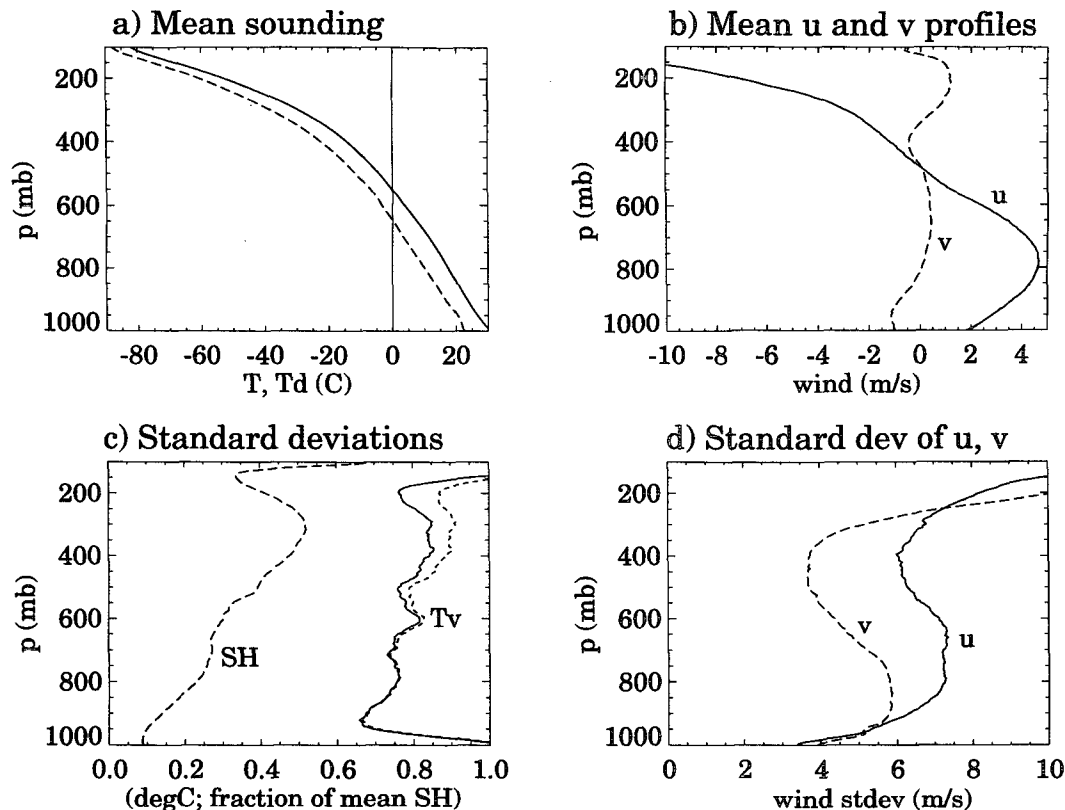## c) Standard deviations

d) Standard dev of u, v

FIG. 4. Means (top row) and standard deviations (bottom row) of sounding parameters for all soundings without any bad data below the 100-mb level. (a) Mean temperature (solid) and humidity (dashed), with humidity expressed as dewpoint. (b) Mean zonal (u, solid) and meridional (v, dashed) winds. (c) Standard deviations of virtual temperature with mean diurnal cycle (Fig. 8) removed (solid, units °C) and included (short dashes) and specific humidity (dashed, expressed as a fraction of the mean). (d) Standard deviations of u (solid) and v (dashed).

vection does manage to penetrate a dry tongue, it will tend to detrain mass into the associated stable layer, destroying the temperature anomaly and possibly creating a "detrainment shelf" of cloud material (discussed in section 6). In this way, midlevel dry tongues may indirectly give rise to midlevel layer clouds, which are frequently observed in the western Pacific region.

2. Data and methods

a. Soundings

The data used in this study come from the eight National Center for Atmospheric Research (NCAR) Cross-chain LORAN Atmospheric Sounding System (CLASS) sites deployed in the western Pacific (map, Fig. 3) during the TOGA COARE field program (Webster and Lukas 1992). More detail on the COARE sounding network may be found in Parsons et al. (1994). Four land sites (Manus, Kapingamarangi, Kavieng, Nauru) and four ships (R/V *Kexue 1*, R/V *Shiyan 3*, R/V *Xiangyanghong 5*, R/V *Moana Wave*) each launched four soundings per day during the four

months of COARE (November 1992 through February 1993). We have used the interpolated dataset at 5-mb resolution. The humidity sensor's long response time at cold temperatures makes the actual resolution of the humidity data considerably coarser than this above about the 400-mb level (Paukkunen 1995). Caution should also be used in interpreting the uncorrected humidity values very near the surface (Miller 1993), but the central results of this paper do not depend on the near-surface moisture values.

Quality control of the data was stringent but primarily automated and consisted of discarding any soundings with missing data or a bad data flag ("99") for pressure, temperature, or humidity anywhere below the 200-mb level (below the 100-mb level in the case of Fig. 4 only). In addition, soundings with any temperature > 320 K, or with a virtual temperature deviation from the mean profile exceeding 5°C between 950 and 200 mb, were excluded. The number of these was small. Visual inspection of time–height images confirmed the reasonableness of all remaining soundings. In all, 2409 of 3005 soundings (80%) were retained. Winds from soundings with a bad wind quality flag

("99") were additionally excluded from the wind composite.

Bulk properties of the COARE sounding dataset are illustrated in Fig. 4 from all soundings with good thermodynamic data to 100 mb. The mean sounding[3] is plotted in Figure 4a. Like all mean tropical soundings, it is not far from a moist adiabat. Dewpoint depressions are 10°C or less throughout the troposphere. The mean zonal wind component (Fig. 4b, solid) indicates mean westerlies up to the 500-mb level and mean easterlies above. Mean meridional winds were weak. The standard deviation of virtual temperature in this dataset is about 0.8°C through the free troposphere, with a slight enhancement at 600 mb, just below the melting level (solid and short-dashed lines, Fig. 4c). The standard deviation of specific humidity (long dashed line, Fig. 4c) increases from 10% of its mean value in the boundary layer to over 50% of its mean value near 300 mb and jumps somewhat sharply to higher values above the melting level (550 mb). The standard deviations of the wind components have midtropospheric minima near 400 mb, with the lower-tropospheric variance peak at a lower altitude for v (dashed) than for u (solid). The variance of v exceeds that of u above the 250-mb level.

b. Radiation codes

Four longwave radiation codes were compared in their responses to humidity variations in the troposphere: the NCAR Community Climate Model (CCM2) code (Hack et al. 1993); the Chou (1991, 1992) code, which was extracted from the radiative–convective software supplied with the Emanuel (1994) textbook; MODTRAN 3 (Berk et al. 1989); and the code described by Fu and Liou (1992). The first two utilize broadband spectral models, while MODTRAN utilizes narrow bands. The Fu and Liou code is based on the correlated k-distribution method.

Figure 5 shows the clear-sky longwave cooling profiles computed by each of these codes for the sounding of Fig. 1b. The codes substantially agree on the cooling profile structure. The biggest differences are in the values near the surface. The cooling at these levels contains substantial contributions from the continuum absorption of water vapor, whose physical basis remains somewhat unclear. To the extent that the codes disagree about this continuum absorbtion, the MODTRAN results are probably the best (Clough et al. 1992). However, MODTRAN 3 is not optimized for cooling rate calculations and proved to be impractical to run. We have instead chosen the CCM2 code for the calcula-
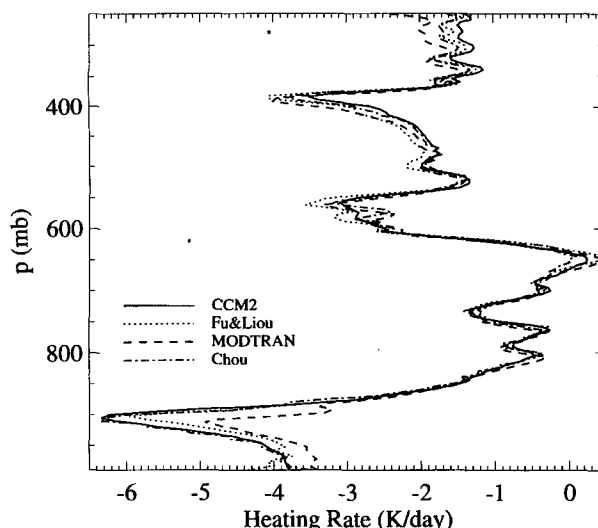

Fig. 5. Comparison of clear-sky longwave cooling rates from four radiation codes for the very dry sounding of Fig. 1b.

tions described herein, primarily for its ease of use. Any one of these codes would be sufficiently accurate for our purposes.

c. Dynamical model

A high vertical resolution linearized primitive equation model is used in this study to compute the density (expressed as temperature) anomalies induced by dry tongue-induced radiative heating rate anomalies. The model uses the vertical spectral representation developed by Fulton and Schubert (1985) to reduce the full three-dimensional linear primitive equations to 64 divergent barotropic equation sets, one for each vertical mode. The linearized horizontal structure equations for each vertical mode are solved by simple time-stepping methods. In this study, a zonally symmetric calculation is performed on an equatorial β plane. This calculation is frictionless and adiabatic except for the specified heating and is linearized about a basic state of rest. The model uses a rigid-lid upper-boundary condition, here applied at the 1-mb level (the stratopause). The solutions shown here are not substantively affected by the altitude of the lid.

3. A composite dry tongue from TOGA COARE soundings

a. Composite method

The first step in developing a composite is to define the central feature of interest. Visual examination of the soundings suggests that dry layers typically have sharply defined bases, where their warmth is particularly concentrated. For this reason, we focus on *humidity drops*, levels where the humidity decreases rapidly

---

[3] In all averaged soundings in this paper, temperature and specific humidity are the averaged variables. These averaged quantities reflect the properties of a hypothetical physical mixture of equal masses of all the air sampled at a given pressure level.

TABLE 1. Frequency of occurrence of humidity drops (layers in which RH decreases with height by more than 15% per 100 m) in the COARE CLASS soundings dataset. Soundings containing one or more of these structures contain about 2.5 on average.

	15%/100-m Humidity drops in the COARE CLASS soundings			
	Number of soundings	Percentage with one or more	Percentage with one or more in $p < 900$	Percentage with one or more in $p < 700$
All OK soundings	2409	46.7	39.8	31.0
Moistest quartile (PWC > 55 kg m^{-2})	529	38.8	33.1	29.9
Cloud-free (RH $< 80\%$ for all $p < 900$)	604	59.6	50.0	36.1

with height. Since we wish to form a composite of humidity drops occurring at many levels in the atmosphere, absolute humidity measures (e.g., mixing ratio, specific humidity) are unsuitable for defining humidity drops.

We considered several criteria for the composite and struggled unsuccessfully to distinguish one single, "natural" humidity variable and vertical coordinate for computing the vertical moisture gradient. One possible pure humidity measure is dewpoint temperature T_d. A dewpoint criterion gives generally similar composite results to those shown below. However, owing to the exponential dependence of humidity on dewpoint, a fixed $d(T_d)/dz$ criterion is more easily realized at low values of T_d. As a result, the composite results in that case (not shown) were dominated by contributions from soundings that are dry at all levels.

Relative humidity is the variable directly measured by the radiosonde sensor. However, relative humidity is not a pure humidity variable: in any given sounding, it depends on the temperature trace as well as the water vapor profile. Because we are seeking to capture in this composite the temperature jump associated with humidity drops, it is imperative that we do not permit the temperature jump to enter the composite definition directly. Therefore, for the composite results here, we

chose a modified definition of relative humidity: the specific humidity (SH) divided by the saturation specific humidity with respect to a plane surface of liquid water computed from the mean temperature profile. In any given sounding, this variable is affected by that sounding's temperature profile only extremely weakly, through its contribution to the mean temperature profile. In practice, this variable is so much like relative humidity that we did not define a new symbol. Where "RH" appears in this paper, it represents this modified relative humidity.

Either pressure or height could be used as the vertical coordinate for evaluating the vertical moisture gradient. When pressure was used, weak uninteresting features in the upper troposphere dominated the composites. For this reason, we chose a height coordinate for computing the moisture gradient, although of course the actual finite differences are taken across 10-mb layers (centered differences in the 5-mb resolution data).

b. Composite results

Table 1 summarizes the climatology of humidity drops with $d(\text{RH})/dz < -15\%/100$ m in this sounding dataset. Of the total 2409 soundings, 47% contain one or more such humidity drops. Some 31% of all soundings have a humidity drop above the 700-mb level. These percentages are somewhat lower for very moist soundings, with precipitable water exceeding 55 kg m^2 (approximately the upper quartile of precipitable water values) and somewhat higher for a similar number of "cloud-free" soundings, defined as those containing no relative humidities (with respect to water) greater than 80% above the 900-mb level. The average number of humidity drops in soundings that contain one or more is 2.5.

1) ALTITUDE DISTRIBUTION OF OCCURRENCE

Figure 6 shows the altitude distribution of humidity drops for $d(\text{RH})/dz$ criteria from $-5\%/100$ m to $-15\%/100$ m. Humidity drops occur at all levels of the troposphere, especially at pressures greater than 400 mb.[4] Prominent peaks in the altitude distribution are at
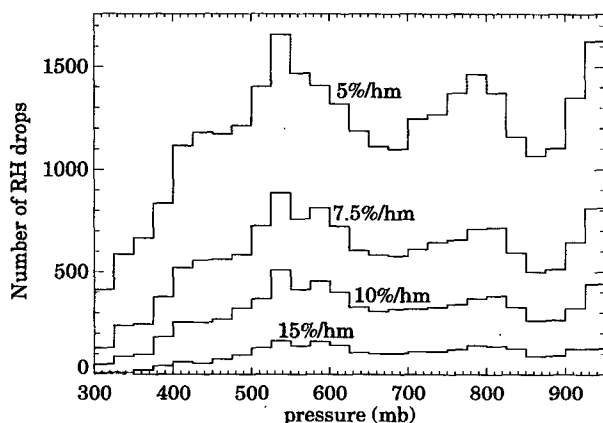
FIG. 6. Altitude distributions of humidity drops with magnitudes exceeding 5%, 7.5%, 10%, and 15% per 100 m based on centered differences in data at 5-mb resolution.

---

[4] Humidity drops in the upper troposphere are poorly sampled ow-

a) composite RH'

b) composite Tv'

c) ΔPθv and ΔPSH
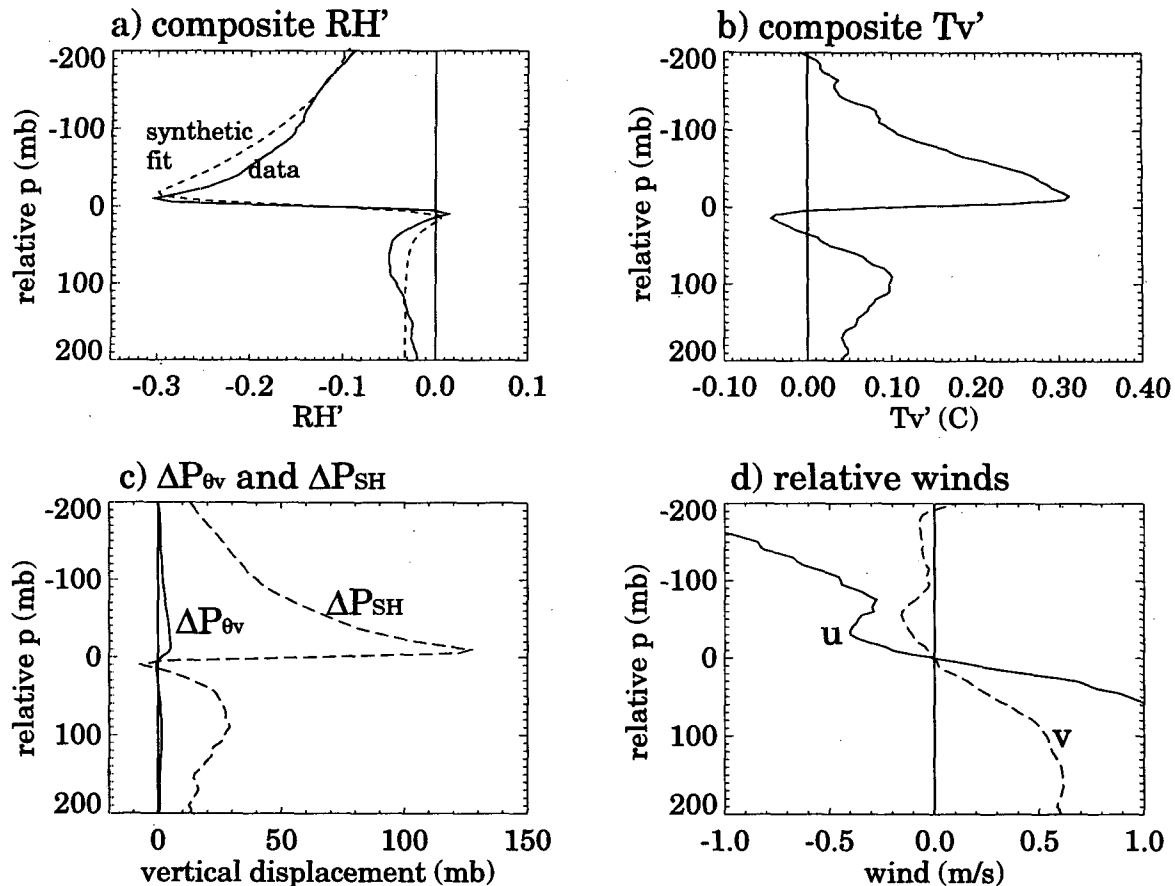
d) relative winds

FIG. 7. The composite dry tongue, defined by humidity drops (see text) exceeding 15% per 100 m, at pressures < 700 mb. All deviations are with respect to the mean sounding of Fig. 4. (a) Humidity deviation RH' (solid) and a synthetic fitted curve (dashed) consisting of two exponential functions. (b) Virtual temperature deviation, T'_v. (c) The equivalent vertical displacement variables $\Delta P_{\theta v}$ and ΔP_{SH}, defined in (1) and (2). (d) Zonal (solid) and meridional (dash) wind components relative to the dry tongue base.

950 mb (the subcloud-layer top), 800 mb (the typical trade inversion level; see, e.g., Schubert et al. 1995 and references therein), and 550 mb (the 0°C level). The altitude distribution in Fig. 6 bears a striking resemblance to the altitude distribution of anomalously stable layers found by Johnson et al. (1995) in this same dataset.

This altitude distribution also resembles the mean profile of convergence in TOGA COARE mesoscale convective systems (Fig. 11a of Mapes and Houze 1995). Perhaps the strong "melting convergence" atop the melting level in MCSs preferentially draws dry air into the COARE radiosonde array at midlevels, as seen in the case examined by Johnson et al. (1995) (days 45–50 in our Fig. 10). However, rawinsonde-derived wind and convergence profile estimates (Fig. 4 and Fig. 13 of Mapes and Houze 1995) do not show systematic evidence of fine structure near the melting

ing to the long response time of the humidity sensor at cold temperatures.

level. In short, the origin and meaning of the observed vertical structure remain somewhat mysterious.

2) Composite structure

Since this dataset is fairly large, a clear composite was obtained using the most stringent criterion of Fig. 6, $d(RH)/dz < -15\%/100$ m. Figure 7 shows the composite humidity, virtual temperature, and relative winds for regions 200 mb below to 200 mb above all such humidity drops above the 700-mb level. We purposely exclude the population of humidity drops near 800 and 925 mb in order to demonstrate that the phenomenon under consideration is not simply the trade inversion. Some 31% (746) of the soundings enter this composite.

Although only a 15%/100 m humidity drop was required, the composite RH' (RH deviation from the all-soundings mean profile) structure shows a drop of over 30% across the composite dry layer base (Fig. 7a). To some extent, this reflects the 10-mb centered difference

a) mean Tv' diurnal variation (all soundings)
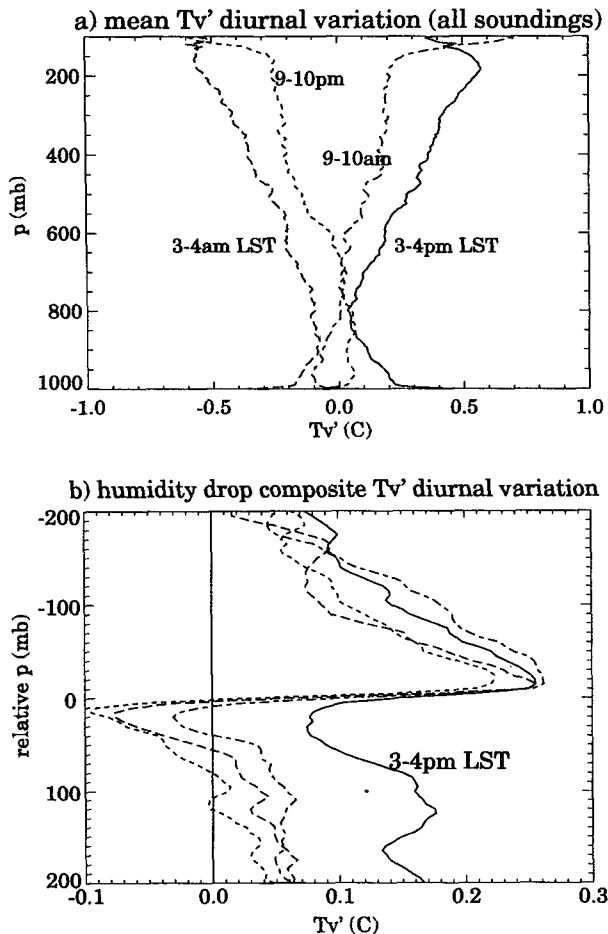

b) humidity drop composite Tv' diurnal variation

FIG. 8. The diurnal variation of virtual temperature: (a) in all analyzed soundings; (b) in the composite dry tongue [as in Fig. 7b, but for $d(RH)/dz < -10\%/100$ m at pressures < 800 mb], with the mean diurnal variation from panel a first removed from the data. Solid: 1500–1600 LST; short dash: 2100–2200 LST; long dash: 0200–0300 LST; long-short dash: 0300–0400 LST.

used to compute the gradient, since 10 mb is about 160 m at the 500-mb level. In the dry layer above the composite humidity drop, RH gradually recovers toward its mean value with an e-folding distance of approximately 125 mb. Immediately below the humidity drop, RH' just touches zero. Other than that, the RH anomaly near this composite humidity drop is negative at all levels, consistent with the fact that humidity drops are more frequent in dry soundings than in moist (Table 1).

Fig. 7b shows the composite T'_v, the virtual temperature deviation from the mean sounding. The dry layer above the composite humidity drop is seen to be anomalously warm by about 0.3°C, atop a very sharp stable layer at the humidity drop. The warm temperature anomaly in the composite dry tongue relaxes back toward zero more rapidly with height than does the low humidity anomaly of Fig. 7a. Aside from a thin layer

of slightly cooler than average temperatures immediately beneath the composite humidity drop, the composite T'_v is positive throughout the 400-mb layer surrounding the composite humidity drop.

(i) Diurnal variability in structure

The diurnal cycle of T'_v in composite dry tongues is shown in Fig. 8b. In order to isolate the dry tongue-associated signal from larger-scale systematic diurnal temperature variations, the mean diurnal cycle of T_v (Fig. 8a) was removed from all soundings. This mean diurnal cycle may contain some biases due to radiative heating of the radiosonde sensor. Nonetheless, it is broadly consistent in amplitude and phase with tidal theory and with previous observations (e.g., Foltz and Gray 1979; Frank 1980 and references therein). In contrast to the symmetry of the mean diurnal cycle, the residual diurnal cycle of T'_v in the vicinity of humidity drops (Fig. 8b) has only one notable feature, an afternoon maximum of temperature in the moist air below the dry layer. This observation suggests that radiation may play a significant role in determining the temperature structure of dry tongues. In order to obtain a clear composite, subdivided into four time-of-day categories, it was necessary in this case to use a less stringent definition of humidity drop: $d(RH)dz < -10\%/100$ m, above the 800-mb level.

(ii) Large-scale aspects of the temperature offset

The positive offset of the T'_v curves in Figs. 7b and 8b reflects the fact that dry-layer occurrence was slightly correlated with deep, large-scale, low-frequency modulations of mean tropospheric temperature.

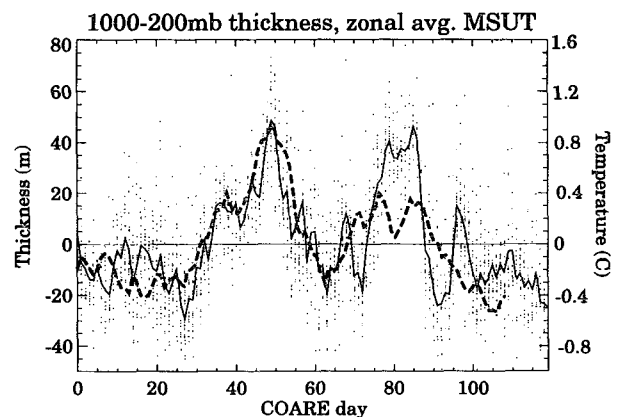### 1000-200mb thickness, zonal avg. MSUT

FIG. 9. Time series during COARE of 1000–200-mb thickness anomaly (scale at left, dots are individual soundings and solid line connects daily means) and temperature anomaly (dashed). Dashed line is a daily tropospheric temperature anomaly (scale at right), zonally averaged around the globe (20°S–20°N) from the Microwave Sounder Unit (MSU, see text), shifted forward in time by 10 days. Day 0 is 1 November 1992.

Figure 9 shows daily mean 1000–200-mb layer thickness anomalies (solid line, daily averages of all the individual sounding thickness anomalies, indicated by dots). Tropospheric thickness varied on an intraseasonal (~40 day) timescale, by some 60 m in the daily mean. Closer examination of the soundings reveals that this thickness anomaly corresponds to a $1°–2°C$ T_v variation, vertically coherent through the troposphere but with larger amplitude in the upper troposphere (not shown).

The near-global scope of this deep low-frequency temperature variation is indicated by its similarity to a global zonally averaged ($20°S–20°N$) daily tropospheric temperature anomaly time series (Fig. 9, dashed line) from the Microwave Sounding Unit (MSU, Spencer and Christy 1992). The quantity plotted is the sum of a lower tropospheric ($1.6T_2 - 0.6T_3$) and an upper tropospheric ($1.35T_3 - 0.35T_4$) temperature index, each with their means over the 120 days of COARE removed. Here subscripts denote MSU channel numbers whose altitude weighting characteristics can be seen in Spencer and Christy (1992). This highly horizontally and vertically averaged temperature anomaly has a peak to peak amplitude exceeding $1°C$.

The zonally averaged MSU time series matches the low-frequency signal in the sounding thicknesses best when shifted backward in time by 10 days (as in Fig. 9). Bantzer and Wallace (1995, personal communication) show that intraseasonal variations in zonally integrated MSU temperature measurements grow as an eastward-propagating wave of warming circles the globe in about 10 days (implying a wave speed of ~45 m s^{-1}). This wave of warming emanates from the enhanced precipitation in the Indo-Pacific warm pool during the active phase of the intraseasonal oscillation (Madden and Julian 1994). These results emphasize that deep (low vertical wavenumber) temperature anomalies must be viewed as a large-scale dynamical variable, not as a local thermodynamic variable. For this reason, we will focus in later sections only on the high vertical wavenumber aspects of the composite T_v' structure of Figs. 7b and 8b.

(iii) Vertical displacements and warm-dry layers

The idea that the composite dry layer might be a result of adiabatic vertical displacements is dispelled by Fig. 7c, which shows the vertical displacement quantities

$$\Delta p_{SH} = \frac{SH'}{\partial(\overline{SH})/\partial p} \quad (1)$$

and

$$\Delta p_{\theta v} = \frac{\theta_v'}{\partial(\overline{\theta_v})/\partial p}. \quad (2)$$

Here an overbar denotes all-sounding mean values, and a prime denotes anomalies from that mean, of SH and virtual potential temperature (θ_v), both of which are conserved in adiabatic vertical displacements. To create the composite humidity deficit with a vertical displacement in a column with the mean vertical gradient of specific humidity would require a downward displacement of over 100 mb. The small temperature anomaly is utterly inconsistent with such a deep adiabatic displacement. To retain its SH values during a 100-mb descent, without retaining its θ_v values, air would have to subside subject to a diabatic cooling, with a magnitude like that of clear-air radiative cooling, for at least a couple of days. Thus, the proximate cause of the appearance of dry air in any particular sounding is probably horizontal advection, as discussed in section 1.

(iv) Composite wind structure

The composite winds, relative to those at the humidity drop, have only a weak signal (Fig. 7d). In part this may be due to cancellation effects (relative wind in the dry layer may come from the northeast in one case, the southwest in another). More to the point, though, the different histories of the air masses above and below the humidity drop do not necessarily imply that they should have different velocities at sampling time. Still, the composite wind profiles do exhibit, in addition to their mean shear, small peaks and overturning structure in, and on the vertical scale of, the composite humidity drop.

3) Time series of dry tongue occurrence

Figure 10 shows time series of the occurrence of humidity drops with $d(RH)/dz < -15\%/100$ m during the four months of TOGA COARE, along with other meteorological time series for reference [see Chen et al. (1996) for an overview of cloud and wind events during TOGA COARE].

The time–height display of humidity drops (Fig. 10a) and the daily number of humidity drops (dashed line on Fig. 10b) show the sporadic nature of their occurrence. The intense dry tongue near 800–900 mb on 10–15 November, which was observed throughout the sounding network, has also been discussed by Parsons et al. (1994) and Numaguti et al. (1995). The latter authors discussed also a dry tongue on COARE day 25. However, it was sampled only by the northernmost of the stations examined here, so it is not outstanding on Fig. 10. The midlevel (~500-mb) dry tongue observed on days 45–47 of Fig. 10 was discussed by Johnson et al. (1995), who showed that its arrival at Nauru was accompanied by a strong northeasterly wind surge at the same levels. The dry tongue apparent on days 95–99 of Fig. 10 was studied by Yoneyama and Fujitani (1995).

a) Time-height display of humidity drops over IFA

b) Precipitable water and number of humidity drops

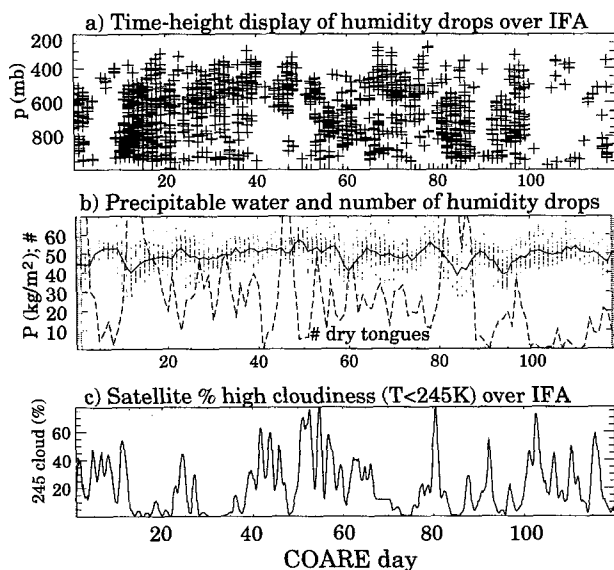c) Satellite % high cloudiness (T<245K) over IFA

COARE day

FIG. 10. (a) Time-height display of humidity drops at the stations making up the COARE Intensive Flux Array (IFA, stations 2–7 on Fig. 3). (b) Daily time series of precipitable water (dots represent individual soundings, line is daily average) and daily number of dry tongues per 32 soundings (dashed). (c) Percent coverage of cloudiness with infrared equivalent blackbody temperature < 245 K, a proxy for deep convection, over a geographical box roughly representing the IFA (4°S–1°N, 152.5°–159°E).

The spikes in the number of humidity drops per day, associated with these strong dry tongue events (dashed line in Fig. 10b), occur against a sizable background of at least some humidity drop occurrences nearly every day of COARE. Humidity drops were more frequent on days with low precipitable water (solid line in Fig. 10c, see also Table 1). More interestingly, humidity drop occurrence is anticorrelated with the satellite-derived high cloudiness (Fig. 10c), a proxy for deep convection. It is particularly interesting that the dry tongue near 500 mb on days 45–48 coincided with a distinct "notch" in the long period of convective activity from days 40 to 70. As discussed in section 6, the composite temperature perturbations associated with dry tongues at this level are not sufficient to prevent convection on the basis of the buoyancy of undilute parcels alone. Perhaps a modeling study of convection using these soundings could elucidate the relative roles of dry air entrainment and buoyancy loss in discouraging deep convection during this period.

4. Clear-air radiative profile calculations

Water vapor is responsible for the major portion of the radiative heating and cooling of the clear troposphere. The profiles of both solar heating and longwave cooling depend strongly upon the humidity profile, but this dependence is nonlocal in the vertical, as explored in sections 4a and 4b. The longwave cooling profile

also depends on the temperature profile to some extent, but because dry tongue humidity variations, expressed as a fraction of their mean value, are so much greater than the associated normalized variations of the Planck function, the humidity profile dependence predominates, as shown in section 4c.

a. Conceptual background: The "cooling to space" approximation

Although we use sophisticated modern radiation codes to compute the radiative heating profiles shown in this paper, it is useful to have a simpler conceptual formulation for understanding their results. One intuitively accessible formulation of the humidity dependence of radiative cooling begins from the "cooling to space" approximation (Rodgers and Walshaw 1966). This approximation ignores the energy exchange with the surface and with adjacent atmospheric layers and is least accurate in the near vicinity of strong moisture or temperature inversions, including the tropopause (Wu 1980). Nevertheless, the approximation can still provide useful qualitative insight into the results portrayed in Figs. 11–14.

Rodgers and Walshaw's equation (3) for longwave cooling to space is

$$Q(z) = B \frac{\partial T(z, \infty)}{\partial z}, \qquad (3)$$

where B is the Planck function and T is the transmission between level z and space ∞. Equation (3) can be rendered more intuitively transparent with the use of an analogy between broadband and monochromatic radiation. If T is related to an optical depth τ, and thereby to an extinction cross section σ (proportional to humidity) by

$$T(z, \infty) \approx \exp(-\tau) \approx \exp\left(-\int_z^\infty \sigma(z')dz'\right), \qquad (4)$$

then (3) can be rewritten as

$$Q(z) \approx B(z)\sigma(z)T(z, \infty). \qquad (5)$$

In words, the radiative cooling at a given level is proportional to the Planck function, the humidity (emitter amount) at level z, and the radiative exposure of level z to the cold environment of space. This exposure factor T depends on the whole column overburden of water vapor so as a result the radiative cooling profile is a nonlocal function of the humidity profile. The special radiative importance of upper-tropospheric water vapor (and cloud) is clearly apparent in this formulation. A more spectrally detailed, yet intuitively accessible, analysis of water vapor cooling in the troposphere was given by Doherty and Newell (1984).

Solar heating of water vapor at any given level is also strongly influenced by the column overburden of water vapor. As a result, there is a distinct symmetry

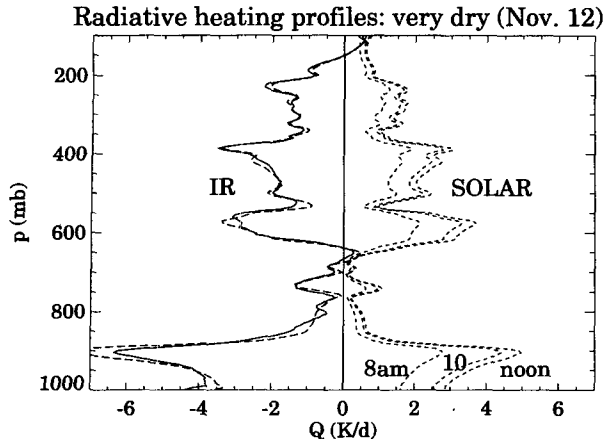Radiative heating profiles: very dry (Nov. 12)

FIG. 11. Solar and longwave (IR) clear-air heating rate profiles for the extreme dry sounding of Fig. 1b, as calculated by the CCM2 radiation code. Solar profiles are shown every 2 hours based on an equinoctal day at the equator. Long dashes indicate the IR cooling rate profile computed when the actual temperature profile is replaced with the mean temperature profile from Fig. 4a.

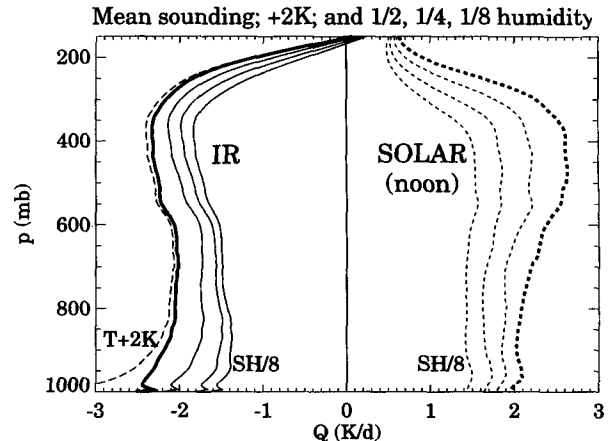Mean sounding; +2K; and 1/2, 1/4, 1/8 humidity

FIG. 12. Clear-air IR and noontime solar heating rate profiles for the mean sounding (heavy lines) and for the mean sounding with $1/2$, $1/4$, and $1/8$ the humidity at all levels (decreasing magnitudes at all levels). Long dashes: IR cooling profile for the mean sounding with temperature increased by 2 K everywhere.

between clear-air longwave cooling and solar heating, as shown in Fig. 11, for the sounding of Fig. 1b. For equatorial solstice conditions, the 24-h average of solar heating is approximately the noontime value divided by π.[5] A decent approximation for daily averaged total clear-air radiative heating is therefore simply to multiply the longwave profile by $(\pi - 1)/\pi$.

b. Sensitivity to deep humidity and temperature variations

One interesting consequence of the exposure factor governing clear-air radiation is that clear-air radiative heating and cooling rates are fairly insensitive to large vertically coherent variations in humidity (cf., Doherty and Newell 1984). Figure 12 shows the computed clear-air heating rates for the mean TOGA COARE sounding (heavy lines) and for that same sounding with $1/2$, $1/4$, and $1/8$ the humidity at all levels (lighter solid and dotted lines). The changes in the heating and cooling rates caused by these humidity changes are larger than the changes associated with a 2 K temperature increase (dashed line), but they are far short of linearly proportional to these rather drastic changes in humidity. Solar heating is somewhat more sensitive to these humidity variations than longwave cooling. This relative insensitivity of longwave cooling to these deep, coherent humidity decreases can be rationalized in terms of (5): at each level, the decrease in emitter

amount is largely compensated by the increased exposure (transmission) to space caused by the humidity decreases in the overlying air.

This compensation allows the radiative cooling of dry air in the subsidence regions of the subtropics to persist long and strongly enough, despite the low humidity, to create extremely low moist static energy air like that seen in Fig. 1b. Notice that in Fig. 11 the dry air is undergoing very little longwave cooling and even some longwave warming near 650 mb.

Figure 13a shows the perturbation to the radiative cooling profile (relative to the mean profile of Fig. 12) for the same mean sounding with its moisture halved only above the 600-mb level. Above that level, the compensation discussed above keeps the cooling rate nearly unchanged. Below the 600-mb level, however, the emitter amount is unchanged while the exposure to space has been increased dramatically. The result is a "bench-shaped" cooling profile, very similar to that
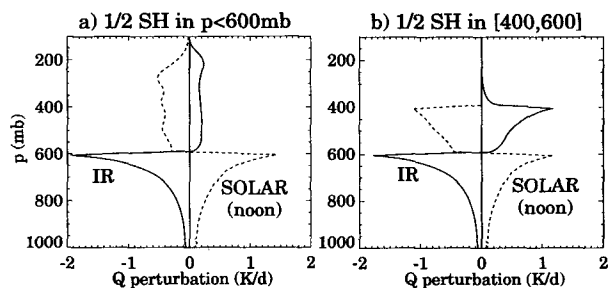

FIG. 13. Clear air radiation experiments with halved humidity, using the CCM2 radiation code. (a) Heating rate devations (relative to Fig. 12) with halved humidity above the 600-mb level. (b) Heating rate devations with halved humidity between 400 and 600 mb.

[5] As pointed out to us by Steven Sherwood, the structure of the solar heating profile is not quite invariant with time of day: there is proportionally more heating higher in the atmosphere at low solar zenith angles.

calculated by Staley (1965) using the Brooks (1950) tabular emissivity method.

Figure 13b shows the results for a "dry sandwich" humidity profile in which the humidity is halved between 600 and 400 mb. Again, the layer immediately below the 600-mb level cools strongly because of its increased exposure to space. Now, however, the air near 400 mb has, relative to the mean sounding, one-half the emitter amount and no extra exposure to space. It therefore experiences a cooling rate about one-half as great as ($\sim$1.2°C/day less than) the air at the corresponding level in the mean sounding. Results are similar for dry layers at other levels in the atmosphere, except that the amplitudes of the cooling anomalies are somewhat greater for dry layers at lower altitudes. Noontime solar heating anomalies are similar in structure but opposite in sign to the longwave cooling anomalies (Fig. 13).

Figure 14 shows the effect of a cloud in the 200–300-mb layer on the "bench" cooling profile of Fig. 13a. This cloud has a liquid water content equal to 10% of the saturation mixing ratio and is just dense enough to be nearly optically black in the infrared. The "bench" shape of the radiative cooling profile remains qualitatively similar, but in this case the underlying mean cooling rate and its humidity-induced anomaly are smaller, the former decreasing gradually with height up to cloud base. The cloud layer itself undergoes strong radiative destabilization and a modest daily mean heating (0.8°C/day in IR, 2.6°C/day in solar) in this case.

c. Relative importance of temperature and humidity variations in warm-dry layers

Humidity variations considerably outweigh temperature variations in terms of their effects on the long-wave cooling profile in dry tongues. This is apparent, in the case of the extreme dry tongue of Fig. 1b, from the dashed line in Fig. 11, which shows the cooling rate calculated from the sounding of Fig. 1b with its temperature profile replaced by the mean temperature profile. To further illustrate this fact, we consider the radiative effects of an adiabatic vertical displacement. As discussed in the introduction, adiabatic vertical displacements represent a far upper limit to the magnitude of temperature anomalies, relative to humidity anomalies, in observed warm-dry layers (Fig. 7c). Dynamically induced vertical displacements are also of interest in their own right, as are the effects of radiation upon them. In particular, this study affords an opportunity to consider the validity of the "Newtonian cooling" approximation frequently used in very simple dynamical models.

Figure 15a shows a vertical displacement profile, with downward displacement (causing warm and dry anomalies) in the upper troposphere above the 500-mb level and upward displacement (causing cool and moist
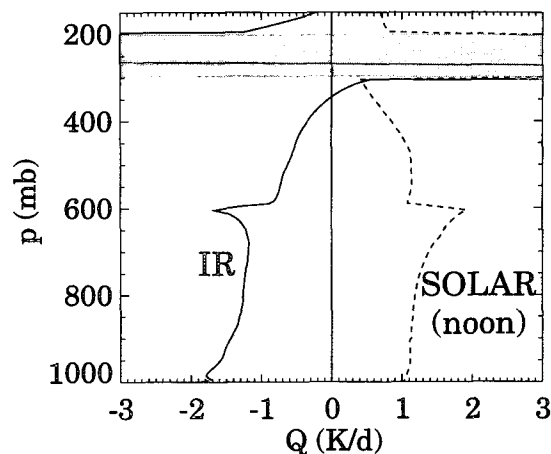

FIG. 14. Heating rates computed for mean sounding with halved humidity above the 600-mb level and with a cloud (overcast) with liquid water content equal to 10% of saturation humidity in the 200–300-mb layer. This cloud is just approaching optical blackness in the infrared. Daily average total heating of the cloud layer is +3.5°C/day (2.6°C/day solar and 0.8°C/day IR).

anomalies) below. This example was chosen because vertical displacements with this profile, and with this sort of amplitude, are caused by tropical mesoscale convective system heating events (Mapes and Houze 1995) and are of interest as contributors to the dynamical modulation of convective instability (Mapes 1993).

This vertical displacement profile was applied to the mean sounding from this study and clear-air radiative cooling rates were computed using the resulting profiles for two cases: one in which the displacement affected the temperature only (TO) and one in which the displacement acted upon both the temperature and humidity fields (TH). Because the amplitude of the displacement is small, the radiative effects of the humidity and temperature changes add almost exactly linearly. Thus, the effects of humidity changes alone can be deduced from the difference between the TO and TH profiles.

Figure 15b shows the perturbations to the longwave cooling profile (again, relative to the mean profile in Fig. 12) in the TO (short dashes) and TH (solid line) cases. The long dashed line shows the "Newtonian cooling" approximation sometimes used in simple dynamical models, given by $Q_N = T'/\tau_N$, where T' is the temperature anomaly and τ_N is a relaxation timescale of 10 days. The Newtonian cooling approximation is quite close to the TO profile: both are zero at the node of the vertical displacement, where $T' = 0$, and the two are comparable in magnitude throughout the troposphere. However, the actual cooling profile anomaly (case TH, solid line) is somewhat greater in amplitude and nearly orthogonal in structure to the TO and Q_N profiles, having its maximum cooling at the 500-mb
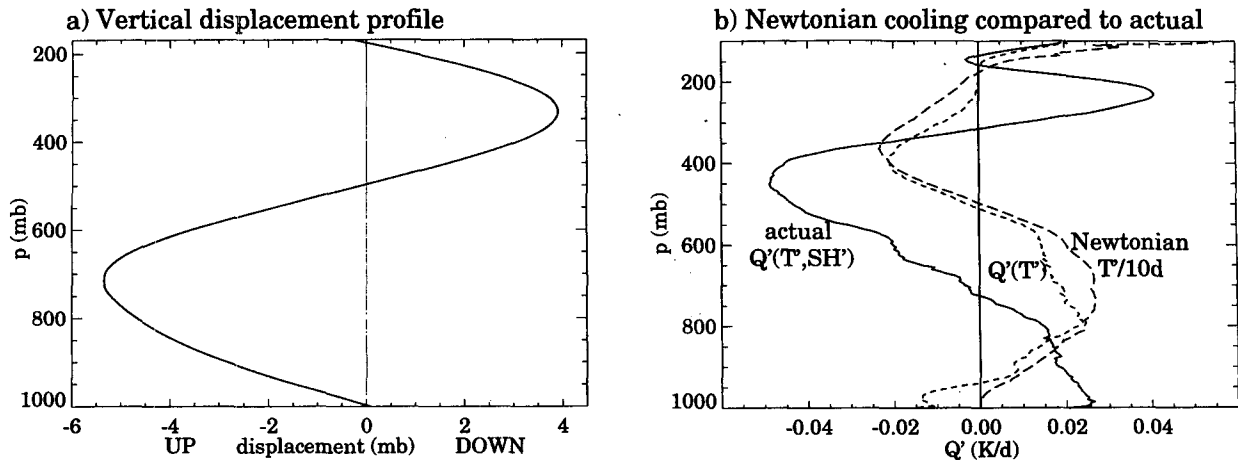
FIG. 15. Infrared cooling rate perturbations, relative to the mean profile (Fig. 12), caused by the vertical displacement shown in (a). (b) The Newtonian cooling approximation with a 10-day time constant (dash); the TO longwave cooling perturbation caused by the displacement-induced temperature perturbations only (dot); and the TH cooling rate perturbation caused by displacement-induced humidity as well as temperature perturbations (solid).

level where the displacement is zero. The increased exposure to space of the air at 500 mb, owing to the drying aloft, causes this maximum in the cooling profile anomaly.

This comparison indicates that humidity variations are somewhat more important to the radiative cooling profile than are temperature variations, even in the case of a purely adiabatic vertical displacement. Again it is evident that the sensitivity of the radiative cooling profile to the humidity profile is quite nonlocal in the vertical. The vertical scale characterizing the nonlocality is ~100–200 mb, as indicated by Fig. 13. Experimentation with individual soundings indicates that, as in Fig. 15, temperature anomalies are generally expressed in the cooling profile much more locally, typically imparting much of the high vertical wavenumber structure to cooling profiles computed from actual soundings.

d. The composite dry tongue cooling profile

The composite humidity variation in Fig. 7a can be idealized with a pair of exponential functions: one to capture the dry layer, with its 125-mb characteristic depth, and one to capture the small moistening below the base:

$$\frac{SH'}{\overline{SH}} = \begin{cases} -0.30 \exp\left(\dfrac{p - p_0}{125\,\text{mb}}\right) - 0.03, & p < p_0 \\[2mm] 0.10 \exp\left(\dfrac{p_0 - p}{20\,\text{mb}}\right) - 0.03, & p > p_0. \end{cases} \tag{6}$$

Here the prime and overbar represent the perturbation and mean profiles, and p_0 represents the pressure level of the humidity drop. This synthetic dry tongue,

smoothed with a 25-mb "boxcar," is plotted on Fig. 7a as a dashed line.

The solid line in Figure 16b shows the daily average solar plus longwave heating profile perturbation that results from this synthetic humidity perturbation to the mean sounding, with the humidity drop level p_0 set to 600 mb. (The profile plotted in Fig. 16 is actually the spectral dynamical model's internal representation of the heating profile, so small Gibbs wiggles due to the spectral truncation can be detected). The magnitude of the heating perturbation is $\pm 0.2°$C day^{-1}. Similar structure obtains for dry tongues at other levels, but with somewhat larger amplitudes for dry tongues at lower altitudes. The perturbation cooling profile is surprisingly symmetric about the 600-mb level, given how asymmetric the humidity structure is.

If acting unopposed, this heating perturbation could create the composite temperature anomaly of Fig. 7b in one day. However, thermally direct circulations may be expected to oppose any localized heating in a fluid.

5. Dynamics relating the heating and temperature anomalies

Staley and Jurica (1968) calculated the radiative evolution of temperature in the vicinity of humidity drops (called "dry inversions" in their paper) using the simplest possible thermodynamic equation $dT/dt = Q_{\text{radiative}}$. Although they included a dry adiabatic adjustment scheme to remove superadiabatic lapse rates, they neglected vertical motion terms in the thermodynamic equation—essentially, an assumption of horizontal homogeneity. However, the dry tongues being considered here are quite limited in horizontal extent. Horizontal radiative heating gradients must therefore drive vertical circulations, which will locally oppose

a) T' (C) @ 3.5 days

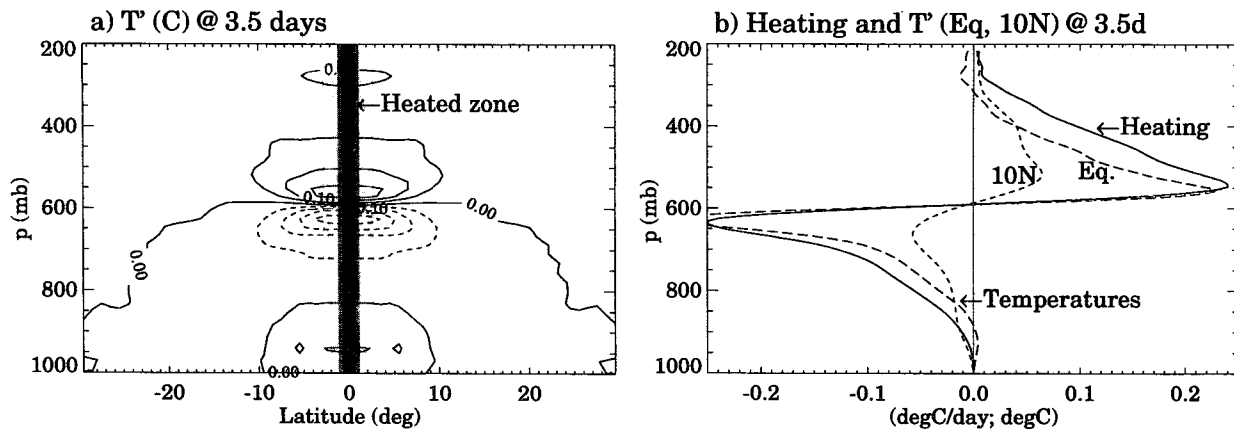## b) Heating and T' (Eq, 10N) @ 3.5d

FIG. 16. The linear temperature perturbation field caused by the imposition of 3.5 days of sustained, zonally symmetric perturbation heating, like that of the composite dry tongue, in an initially uniform, motionless atmosphere with realistic stratification on a β plane. (a) Temperature in the latitude-pressure plane. Shading illustrates the $\cos^2$(latitude) horizontal structure of the imposed heating, which is confined between 3°N and 3°S. (b) Equatorial profiles of heating (solid) and temperature (long dash) after 3.5 days and temperature at latitude 10° after 3.5 days (short dash).

the $Q_{radiative}$ term in the equation for temperature and at the same time change the temperature elsewhere in the atmosphere.

One complication is that the radiative cooling perturbations caused by dry tongues exist against a background of $\sim 1.5°$–$2°C$ day^{-1} net cooling of the entire troposphere. If operating unopposed, this mean cooling would move the temperature more than two standard deviations away from its mean value (Fig. 4) in a day. Apparently, radiative cooling in the Tropics is rather closely balanced by subsidence warming. Another indication of the ubiquity of radiatively driven subsidence is the ~ 400 m day^{-1} downward motion of features in specific humidity profiles (which may be viewed as passive tracers, in suppressed conditions when convective vertical transports are weak) found by both Yoneyama and Fujitani (1995) and Numaguti et al. (1995). The supply of high potential temperature air aloft for this deep subsidence, and the sink of low potential temperature air at low levels, is precipitating deep convection, which may be quite distant, with large-scale circulations transporting the necessary entropy horizontally.

This section is meant to illustrate how high vertical wavenumber features of the heating profile in a localized dry tongue lead to sharp, locally trapped temperature features like those observed in the sounding composite, while lower vertical wavenumber components cause temperature anomalies with larger horizontal scale and correspondingly smaller amplitude. For long timescales in a rotating fluid, the ratio of horizontal to vertical scales is expressed in the familiar concept of vertical wavenumber-dependent Rossby deformation radii. But similar aspect ratio considerations hold for transient heat sources as well (e.g., Nicholls et al. 1991; Bretherton 1993; Mapes 1993). The lowest vertical

wavenumbers of tropospheric radiative cooling and convective heating participate in a distributed radiative–convective near-equilibrium, at planetary scales, as discussed above and in section 3b.2(ii). We avoid the necessity of simulating this large-scale general circulation of the Tropics by modeling only the heating, circulation, and temperature *perturbations* associated with an idealized dry tongue.

a. Why is T' sharper and shallower than Q'?

Consider the dynamical response to a zonally symmetric dry tongue-like radiative heating profile anomaly, with horizontal structure given by $\cos^2(\pi/2 \times$ latitude$/3°)$ (with 333-km full-width at half amplitude), centered on the equator, in a realistically stratified atmosphere linearized about a state of rest. The heating profile used in this experiment is a slightly smoothed daily mean anomalous heating, computed from the synthetic humidity drop shown as a dashed line in Fig. 7a, and is plotted in Fig. 16b as it is internally represented in the dynamical model. In this idealized model run, the heating begins suddenly and acts constantly for 3.5 days, at which time the temperature field is evaluated.

The latitude–height temperature perturbation field after 3.5 days is shown in Fig. 16a. The temperature anomaly contours extend throughout the plotted domain, far beyond the near-equatorial heated zone, delineated by vertical lines.

Temperature anomaly profiles at the equator and 10°N are shown in Fig. 16b, with the heating rate profile plotted for comparison. Both these temperature profiles qualitatively resemble the heating profile, but the equatorial profile, inside the heated region, is quite sharply localized (in the vertical) in the vicinity of the humidity drop at 600 mb. In other words, it is relatively

enriched in the highest vertical wavenumbers, which are trapped in the vicinity of the heating. By contrast, the temperature perturbation profile at 10°N is enriched in low wavenumbers, with temperature values that actually exceed those of the equatorial profile at some levels far from the 600-mb level.

The temperature profile at 10°N is composed of only those vertical wavenumbers characterized by gravity wave speeds faster than about 777 km/3.5 d = 2.6 m s^{-1}. In a hydrostatic stratified fluid with constant buoyancy frequency N, the wave speed c is related to vertical wavenumber m by $c = N/m$, so for a typical value of $N = 10^{-2}$ s^{-1}, it follows that vertical wavelengths smaller that about a kilometer have been dynamically filtered out of the 10°N profile and are correspondingly present with enhanced amplitude within the heated region nearer the equator.

The magnitude of the equatorial temperature anomaly in Fig. 16b, 0.4°C peak to peak, is comparable to that observed in the sounding composite from which the humidity and thereby the radiative heating rate were derived. This result was ensured by the choice of the 333-km width of the dry tongue and the 3.5-day evaluation time. A major effect of dynamics, then, is simply to moderate the development of temperature anomalies in response to localized heating: it took 3.5 days for this 0.2°C day^{-1} heating anomaly to create a local 0.2°C temperature anomaly.

The width and evaluation time choice is consistent with observations. A considerable amount of humidity structure on the few hundred kilometer scale, even aside from the main dry tongue, can be seen in Fig. 3, as well as in other precipitable water maps (e.g., Plate 1 of Sheu and Liu 1995). A 3–4-day lifetime for dry tongues was also indicated by the studies of Numaguti et al. (1995) and Yoneyama and Fujitani (1995). In short, radiation, in combination with dynamics, acting on dry tongues of typical width and duration, can quite feasibly explain the observed composite thermal structure of dry tongues, including the temperature anomaly's confinement near the humidity drop.

6. Implications of dry tongues for convection

Why deep tropical convection occurs when and where it does remains substantially unknown, notwithstanding the bland statement that convection tends preferentially to occur over warm moist surfaces. Dry tongues can alter the fate of would-be penetrating convective clouds in two ways. The anomalously warm layer directly decreases the buoyancy of any parcel within it, by definition. In addition, mixing by the parcel with the dry tongue air can inhibit buoyant convection. This section considers how dry tongues, with the accompanying thermal anomalies at their bases, might affect the viability of deep convective clouds and hence play a role in modulating the distribution of convection.

a. Parcel buoyancy in soundings with dry tongues at various levels

As a preliminary assessment of these effects, Fig. 17 shows the profiles of moist static energy h and saturation moist static energy h^* for mean soundings containing dry tongues at various levels. Both the dryness and the warmth of dry tongues are captured by this diagram: the dryness leads to minima in the h profiles, while the warmth is seen as maxima in the h^* profiles. Surface parcels, rising undiluted through the atmosphere, are represented by vertical lines in Fig. 17. At any level at which the parcel is saturated, its temperature difference from its environment is indicated by its position relative to the environmental h^* profile. Temperature differences from the environmental sounding are ruled off in thin lines every 0.5°C in the area between the parcel h and environmental h^* profiles.

These plots also offer a qualitative view of the potential effects of mixing on buoyancy because h is a nearly linearly mixing quantity (see the definition of h in footnote 2). If a parcel entrains 10% of its mass in environmental air at some height, its h profile will move 10% of the distance toward the environmental h profile line. If the mixture is still saturated, its temperature difference from the environment may still be checked with reference to the environmental h^* profile, as before.

The effect of the trade inversion on convection is illustrated by the average of all the soundings with a 15%/100 m dry layer base between 780 and 800 mb (Fig. 17b). In these cases, the stability anomaly associated with the humidity drop constitutes a strong "cap" on the trade cumulus layer, effectively preventing deeper convection (e.g., Riehl 1954). Plots like these were the basis of the conclusion of Kloesel and Albrecht (1989) that "low-level inversions apparently play a critical role in regulating convection over a broad region of the Tropics."

The mean of 49 soundings with dry layer bases in the 680–700-mb layer, near the minimum in the frequency distribution with altitude (Fig. 6), is plotted in Fig. 17c. In this case, the dry tongue constitutes a substantial "notch" in a surface parcel's positive buoyancy profile, if not an actual cap to convection. The dry air above 700 mb is apparent as a minimum in the h profile. A relatively small mixing fraction of this dry air could have a strong negative effect on parcel buoyancy.

In the case of dry layer bases in the 580–600-mb layer (Fig. 17d), the importance of the dry tongues to convective viability is less clear but still deserves recognition. Even if the virtual warmth of a layer is insufficient to actually negate the buoyancy of a penetrating buoyant cloud, environmental temperature perturbations that decrease with height (like the T_v profile within the dry air in Fig. 7b) can still cause entrainment (Bretherton and Smolarkiewicz 1989). A hypothesized
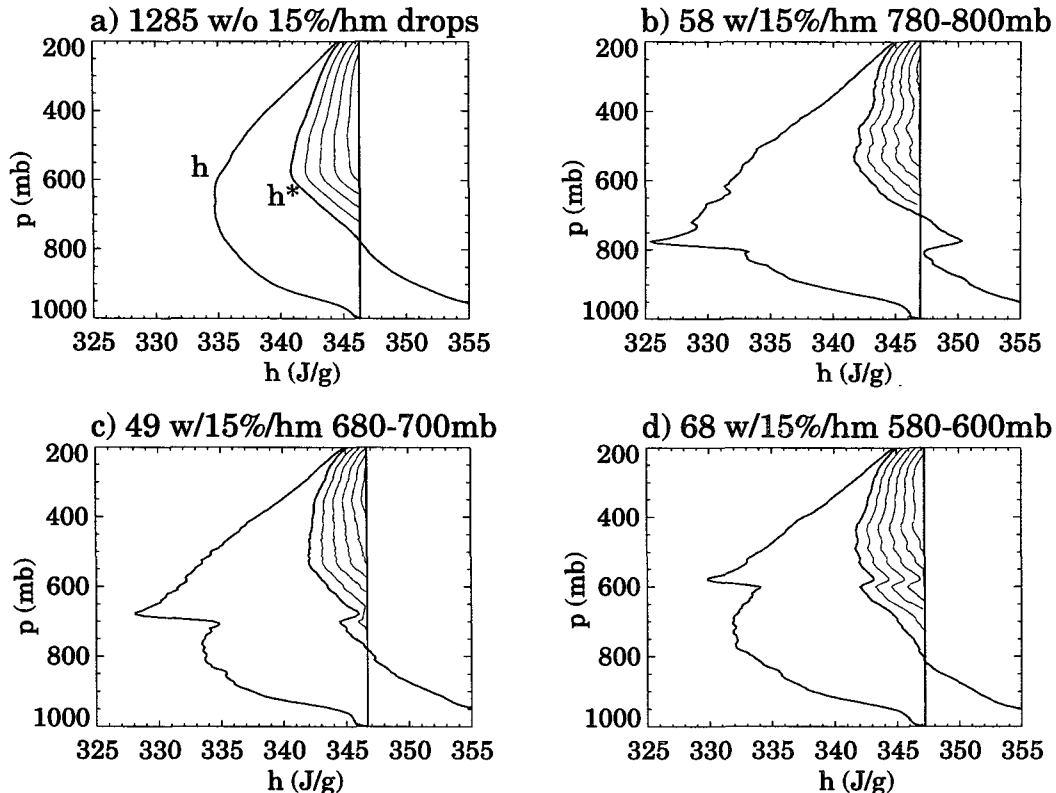
a) 1285 w/o 15%/hm drops

b) 58 w/15%/hm 780-800mb

c) 49 w/15%/hm 680-700mb

d) 68 w/15%/hm 580-600mb

FIG. 17. Moist static energy h (defined in footnote, section 1) and saturation moist static energy h^* for various mean soundings: (a) 1285 soundings, which lack a 15%/100 m humidity drop at any level, (b) 58 soundings with humidity drops in the 780–800-mb layer; (c) 49 soundings with humidity drops in the 680–700-mb layer; (d) 68 soundings with humidity drops in the 580–600-mb layer. Vertical lines mark the h value of air at 1000 mb (sensitive to low-level humidity, which may be in error in this dataset). Light ruling indicates temperature differences between an undilute parcel from 1000 mb and the environment in 0.5°C increments.

mechanism is that buoyancy gradients across a parcel drive subparcel-scale mixing eddies (Taylor and Baker 1991). By entraining "gulps" of dry air, these eddies could indirectly destroy the buoyancy of a convective cloud penetrating a dry tongue.

b. Dry tongues, convective detrainment, and layer clouds

Conversely, when convection does manage to penetrate a stratification anomaly such as that at the base of a dry tongue, it may detrain an anomalous amount of mass into the stable layer (Bretherton and Smolar-kiewicz 1989; Taylor and Baker 1991; Raymond and Blyth 1992). Mapes and Houze (1995, their sections 4c.3 and 6a) attributed the systematic, anomalous mesoscale divergence observed at 3-km altitude in one well-sampled convective rainband to a stratification anomaly not unlike, though of some five times larger amplitude than, the composite dry tongue thermal anomaly of Fig. 7b.

Detrainment of convective cloud mass flux into dry tongue-related stratification anomalies may cre-

ate layer clouds—the detrainment "shelves" frequently observed in convecting environments. If so, one might hypothesize that there should be more cloudiness at levels in which humidity drops are frequently observed. Figure 18 shows the vertical distribution of the frequency of nearly saturated layers (a proxy for cloud) in the present sounding dataset. This altitude distribution shows considerable similarity to that of humidity drops (Fig. 6), consistent with the above hypothesis.

Of course, this similarity may indicate that the humidity and temperature structures being examined in this paper are somehow formed by cloudy layers (the term "cloud fossils" was suggested by Steven Sherwood), rather than vice versa. If a deep tropospheric slab containing a layer cloud subsides far enough to evaporate the cloud, the result is a moist-beneath-dry structure, with a stable layer separating the moist and dry air. This is certainly a fair qualitative description of the composite structure seen in Fig. 7: the layer immediately beneath a composite humidity drop does contain a local maximum in humidity (Fig. 7a) and in moist static energy (Fig. 17). However, there is little

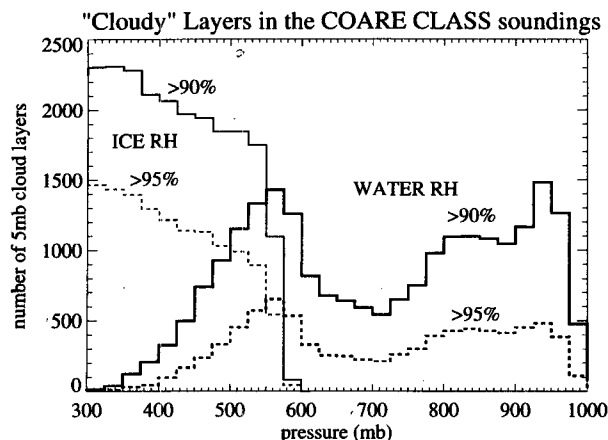"Cloudy" Layers in the COARE CLASS soundings

FIG. 18. Altitude distribution of layers with humidity exceeding 90% (solid) or 95% (dashed), intended as a proxy for cloudy layers. Relative humidity (RH) with respect to ice is indicated in lighter lines above the 0°C level.

doubt that dry air advection is responsible for the very intense dry tongues, as seen in Figs. 1–3 and in Parsons et al. (1994), Numaguti et al. (1995), Yoneyama and Fujitani (1995), and Johnson et al. (1995). Even in the composite picture, the dry layers above elevated humidity drops usually constitute distinct absolute minima in moist static energy (Fig. 17b,c), implying an out of column origin.

No doubt the humidity drops studied here include both advective dry tongue bases and cloud fossils, and possibly other phenomena as well. Anomalously stable layers, with an altitude distribution very similar to those in Figs. 6 and 18, are even more general than the humidity drops studied here (Johnson et al. 1995). Perhaps those authors have identified the most important challenge: to understand why all these interrelated phenomena have a distinct maximum in frequency near the melting level.

c. Radiative–convective balance

Finally, we note that the convective detrainment into dry tongue-associated stable layers discussed above also has an interpretation in terms of convective heating. Consider the schematic Fig. 19, which indicates the temperature and heating perturbations associated with a dry tongue stability anomaly, as perturbations to the deep (low vertical wavenumber) general circulation of the tropical atmosphere. On the largest scale, nearly ubiquitous deep radiative cooling (e.g., Figs. 12, 14) is balanced rather closely by subsidence warming. The closeness of this balance is indicated by the small standard deviation of temperature in Fig. 4c, while the rapidity with which deep-layer mean temperature variations are homogenized throughout the Tropics is illustrated by Fig. 9 [section 3b.2(ii)]. Deep convective

heating, considerably more localized in space and time than the radiative cooling, carries the upward cross-isentropic mass transport that ultimately sustains this deep subsidence.

The shallow (high vertical wavenumber) anomalous mass detrainment into an environmental stable layer is part of a shallower vertical circulation, as indicated on Fig. 19. In the convection, there is anomalous net upward mass flux in the layer in which the environment is anomalously cool and anomalous net downward mass flux in the layer in which the environment is warm. This circulation constitutes a convective heating anomaly that tends to destroy these environmental temperature anomalies, as may be appreciated from consideration either of the implied anomalous net latent heating in the convection or of the corresponding dry vertical motions outside the convection. Evidence for, and consequences of, this negative feedback between environmental temperature and convective heating are discussed in Mapes and Houze (1995).

These processes are consistent with the idea that a radiative–convective thermal balance prevails for high vertical wavenumber anomalies, as well as for the more familiar deep processes determining the mean stratification of the atmosphere (e.g., Manabe and Strickler 1967). In this scenario, the temperature field is the medium of communication between radiative and convective diabatic processes.

7. Summary and conclusions

Dry layers, with sharply defined bases (the "humidity drops" used here as the basis of the composite), are common elements in sounding datasets, even in the climatologically humid western Pacific region. Conserved variable analyses and case studies (Numaguti et al. 1995; Yoneyama and Fujitani 1995) indicate that differential advection is the proximate cause of these

convective heating anomalies   no convection: shallow
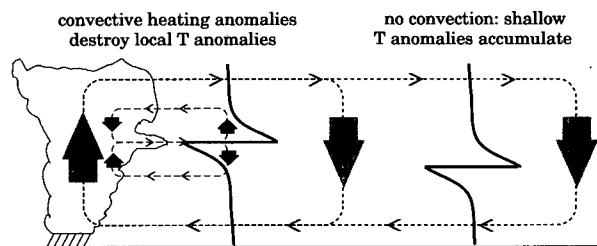destroy local T anomalies   T anomalies accumulate

FIG. 19. Schematic picture of the role of dry tongues in the tropical climate. Deep convective heating in one region supplies the upward cross-isentropic mass flux (upward large arrow) sustaining the subsidence (downward large arrows) that balances deep (low vertical wavenumber) components of radiative cooling. Outside of convective regions, dry tongues create high-vertical-wavenumber stability anomalies like those studied here (heavy lines). When convection encounters these stable layers, it detrains mass (smaller vertical arrows and light dashed circulation), thus heating the cool anomaly and cooling the warm anomaly.

dry layers, which we therefore refer to as dry tongues. Despite the relatively small horizontal scale of each realization, dry tongues are frequent enough to be climatologically important (Table 1). This paper takes a statistical approach to understanding the origins and dynamics of dry tongues.

Figure 7 shows the composite temperature and moisture structure in the vicinity of "humidity drops" (places where humidity decreases rapidly with height, such as at the base of a dry tongue). The composite dry layer is anomalously warm, especially near its base, while the layer below it exhibits slight moist and cool anomalies. In other words, a sharp stable stratification separates dry tongues from the moist air below. Quantitative examination of these humidity and temperature anomalies indicates that the composite dry tongue is far too dry (or, alternatively, not warm enough) to be explicable as an adiabatic vertical displacement (Fig. 7c).

The warmth of the composite dry tongue (i.e., the positive offset of the temperature seen in Figs. 7b and 8b) was shown to reflect a slight, possibly coincidental, correlation between dry tongue occurrence and a global-scale intraseasonal oscillation in deep-layer temperatures (Fig. 9). This result emphasizes that deep temperature anomalies are under very large-scale dynamical control, such that only high vertical wavenumbers in the profile of virtual temperature can be attributed to local thermodynamic processes. Even the relatively shallow radiative heating anomaly associated with a dry tongue affects the temperature profile over an area considerably larger than the dry tongue itself (Fig. 16).

The altitude distribution of humidity drops shows, in addition to peaks atop the subcloud and trade cumulus layers, a peak centered on 550 mb near the 0°C level (Fig. 6; see also Johnson et al. 1995). However, dry tongues are most frequently observed in low-humidity soundings (Table 1), presumably far from the local occurrence of strong hydrometeor melting.

The effect of a dry tongue on the radiation profile is to cause anomalous longwave heating in the dry air above an anomalous cooling of the top of the underlying moist air. The sense of this radiative heating anomaly is such as to stabilize the dry tongue base. Solar radiation has an opposite, that is, destabilizing, effect but is smaller in magnitude when averaged throughout the day. An afternoon elevation of the moist layer temperature, that is, a minimum of static stability of the stable layer, is observed in the data composite (Fig. 8b). The thermal structure of dry tongues, including the confinement of warming near the base of the dry air, can be well explained by the dynamical effects of the radiative heating anomalies they induce, assuming typical dry tongue widths of a few hundred kilometers and lifetimes of 3–4 days. These scales are consistent with those estimated in the case studies of Numaguti et al. (1995) and Yoneyama and Fujitani

(1995) and are deduced from satellite precipitable water imagery (Fig. 3; Plate I of Sheu and Liu 1995).

The temporal distribution of dry tongue occurrence at these sounding sites (Fig. 10) bears a distinct anticorrelation with convection, as noted by Numaguti et al. (1995) and Yoneyama and Fujitani (1995). Dry tongues at the trade inversion level (800 mb) typically present an impassible obstacle to would-be convective clouds (Fig. 17b). But even at higher altitudes, where warm dry tongues may not entirely negate the buoyancy of unmixed parcels, the entrainment of dry tongue air, perhaps enhanced by the stratification anomaly itself, could still be fatal to the marginal cloud. Since convection is, in turn, the source of moisture in the troposphere, dry tongues and their radiatively maintained stable layers may organize the persistence of the absence of convection.

Convection preferentially detrains into stable layers such as those associated with dry tongues (Bretherton and Smolarkiewicz 1989). This detrainment of cloudy air may give rise to midlevel cloud decks (Fig. 18). Such clouds can affect not only atmospheric radiative heating profiles but also the net radiation balance of the earth–atmosphere system in the Tropics. The convective heating anomaly implied by this detrainment tends to destroy the temperature structure that causes the detrainment. We speculate that this is how the high-vertical–wavenumber parts of long-term climatic balance between radiative cooling and convective heating in the atmosphere are realized.

In summary, chaotic advection in the presence of intense subtropical–tropical humidity gradients and the sporadic nature of convective moisture sources inevitably gives rise to a humidity field with abundant fine structure in both the horizontal and vertical directions. Since water vapor is a powerful greenhouse gas, thermal fine structure is quickly generated by the humidity structure. The combination of humidity and temperature structure can affect the distribution and properties of convection and convectively generated cloudiness.

two anonymous reviewers helped us refine the presentation.

REFERENCES

Berk, A. L., L. S. Bernstein, and D. C. Robertson, 1989: MODTRAN: A Moderate Resolution Model for LOWTRAN7. Rep. GL-TR-89-0122, Air Force Geophysics Lab, Bedford, MA, 42 pp.

Bretherton, C. S., 1993: The nature of adjustment in cumulus cloud fields. *The Representation of Cumulus Convection in Numerical Models of the Atmosphere*, K. A. Emanuel and D. J. Raymond, Eds., *Meteor. Monogr.*, vol. 24, No. 46, Amer. Meteor. Soc., 63–74.

——, and P. K. Smolarkiewicz, 1989: Gravity waves, compensating subsidence, and detrainment around cumulus clouds. *J. Atmos. Sci.*, **46**, 740–759.

Brooks, D. L., 1950: A tabular method for the computation of temperature change by infrared radiation in the free troposphere. *J. Meteor.*, **7**, 313–330.

Chen, S. S., R. A. Houze Jr., and B. E. Mapes, 1996: Multiscale variability of deep convection in relation to large-scale circulation during TOGA-COARE. *J. Atmos. Sci.*, in press.

Chou, M.-D., 1992: A solar radiation model for use in climate studies. *J. Atmos. Sci.*, **49**, 762–772.

——, D. P. Krats, and W. Ridgway, 1991: Infrared radiation parameterization in numerical climate models. *J. Climate*, **4**, 424–437.

Clough, S. A., M. J. Iacono, and J.-L. Moncet, 1992: Line-by-line calculations of atmospheric fluxes and cooling rates: Application to water vapor. *J. Geophys. Res.*, **97**(D14), 15 761–15 785.

Doherty, G. M., and R. E. Newell, 1984: Radiative effects of changing atmospheric water vapor. *Tellus*, **36B**, 149–162.

Emanuel, K. A., 1994: *Atmospheric Convection*. Oxford University Press, 580 pp.

Foltz, G. S., and W. M. Gray, 1979: Diurnal variation in the troposphere's energy balance. *J. Atmos. Sci.*, **36**, 1450–1466.

Frank, W. M., 1980: Modulation of the net tropospheric temperature during GATE. *J. Atmos. Sci.*, **37**, 1056–1064.

Fu, Q., and K. N. Liou, 1992: On the correlated k-distribution method for radiative transfer in nonhomogeneous atmospheres. *J. Atmos. Sci.*, **49**, 2139–2156.

Fulton, S. R., and W. H. Schubert, 1985: Vertical normal mode transforms: Theory and application. *Mon. Wea. Rev.*, **113**, 647–658.

Hack, J., B. A. Boville, B. P. Briegleb, J. T. Kiehl, P. J. Rasch, and D. L. Williamson, 1993: Description of the NCAR Community Climate Model (CCM2). NCAR Technical Note NCAR/TN-382+STR, Boulder, CO, 46–61.

Kloesel, K. A., and B. A. Albrecht, 1989: Low-level inversions over the tropical Pacific—thermodynamic structure of the boundary layer and the above-inversion moisture structure. *Mon. Wea. Rev.*, **117**, 81–101.

Madden, R. A., and P. R. Julian, 1994: Observations of the 40–50-day tropical oscillation—a review. *Mon. Wea. Rev.*, **122**, 814–837.

Manabe, S., and R. F. Strickler, 1964: Thermal equilibrium of the atmosphere with a convective adjustment. *J. Atmos. Sci.*, **21**, 361–385.

Mapes, B. E., 1993: Gregarious tropical convection. *J. Atmos. Sci.*, **50**, 2026–2037.

——, and R. A. Houze Jr., 1995: Diabatic divergence profiles in western Pacific mesoscale convective systems. *J. Atmos. Sci.*, **52**, 1807–1828.

Miller, E., 1993: TOGA COARE Integrated sounding system data report—Vol. I, surface and sounding data. NCAR SSSF Rep., 41 pp.

Namias, J., 1936: Structure and maintenance of dry-type moisture discontinuities not developed by subsidence. *Mon. Wea. Rev.*, **64**, 351–358.

Nicholls, M. E., R. A. Pielke, and W. R. Cotton, 1991: Thermally forced gravity waves in an atmosphere at rest. *J. Atmos. Sci.*, **48**, 1869–1884.

Numaguti, A., R. Oki, K. Nakamura, K. Tsuboki, N. Misawa, T. Asai, and Y.-M. Kodama, 1995: 4–5-day-period variations and low-level dry air observed in the equatorial western Pacific during the TOGA-COARE IOP. *J. Meteor. Soc. Japan*, **73**, 267–290.

Parsons, D., W. Dabberdt, H. Cole, T. Hock, C. Martin, A.-L. Barrett, E. Miller, M. Spowart, M. Howard, W. Ecklund, D. Carter, K. Gage, and J. Wilson, 1994: The integrated sounding system: Description and preliminary observations from TOGA-COARE. *Bull. Amer. Meteor. Soc.*, **75**, 553–569.

Paukkunen, A., 1995: Sensor heating to enhance reliability of radiosonde humidity measurement. *Ninth Symp. on Meteorological Observations and Instrumentation*, Charlotte, NC, Amer. Meteor. Soc., 65–69.

Petty, G. W., 1994: Physical retrievals of over-ocean rain rate from multichannel microwave imagery. Part II: Algorithm implementation. *Meteor. Atmos. Phys.*, **54**, 101–121.

Raymond, D. J., and A. M. Blyth, 1992: Extension of the stochastic mixing model to cumulonimbus clouds. *J. Atmos. Sci.*, **49**, 1968–1983.

Riehl, H., 1954: *Tropical Meteorology*. McGraw-Hill, 392 pp.

Rodgers, C. D., and C. D. Walshaw, 1966: The computation of infrared cooling rate in planetary atmospheres. *Quart. J. Roy. Meteor. Soc.*, **92**, 67–92.

Schubert, W. H., P. E. Ciesielski, C. Lu, and R. H. Johnson, 1995: Dynamical adjustment of the trade wind inversion layer. *J. Atmos. Sci.*, **52**, 2941–2952.

Sheu, R.-S., and G. Liu, 1995: Atmospheric humidity variations associated with westerly wind bursts during TOGA COARE. *J. Geophys. Res.*, in press.

Spencer, R. W., and J. R. Christy, 1992: Precision and radiosonde validation of satellite gridpoint temperature anomalies. Part I: MSU channel 2. *J. Climate*, **5**, 847–857.

Staley, D. O., 1965: Radiative cooling in the vicinity of inversions and the tropopause. *Quart. J. Roy. Meteor. Soc.*, **91**, 282–301.

——, and G. M. Jurica, 1968: Radiative modification of selected vertical temperature distributions. *Quart. J. Roy. Meteor. Soc.*, **94**, 310–317.

Taylor, G. R., and M. B. Baker, 1991: Entrainment and detrainment in cumulus clouds. *J. Atmos. Sci.*, **48**, 112–121.

Webster, P. J., and R. Lukas, 1992: TOGA-COARE: The Coupled Ocean–Atmosphere Response Experiment. *Bull. Amer. Meteor. Soc.*, **73**, 1377–1416.

Wu, M.-L. C., 1980: The exchange of infrared radiative energy in the troposphere. *J. Geophys. Res.*, **85**, 4084–4090.

Yoneyama, K., and T. Fujitani, 1995: The behavior of dry westerly air associated with convection observed during the TOGA-COARE R/V Natsushima cruise. *J. Meteor. Soc. Japan*, **73**, 291–304.

Zipser, E. J., 1977: Mesoscale and convective-scale downdrafts as distinct components of squall-line structure. *Mon. Wea. Rev.*, **105**, 1568–1589.